

Narrow-band Imaging in the CN Band at 388.33 nm

Han Uitenbroek and Alexandra Tritschler

National Solar Observatory/Sacramento Peak*, P.O. Box 62, Sunspot, NM 88349, U.S.A.
e-mail: huitenbroek@nso.edu, atritschler@nso.edu

October 1, 2018

ABSTRACT

Aims. We promote the use of narrow-band (0.05 — 0.20 nm FWHM) imaging in the molecular CN band head at 388.33 nm as an effective method for monitoring small-scale magnetic field elements because it renders them with exceptionally high contrast.

Methods. We create synthetic narrow-band CN filtergrams from spectra computed from a three-dimensional snapshot of a magnetohydrodynamic simulation of the solar convection to illustrate the expected high contrast and explain its nature. In addition, we performed observations with the horizontal slit spectrograph at the Dunn Solar Tower at 388.3 nm to experimentally confirm the high bright-point contrast, and to characterize and optimize the transmission profile of a narrow-band (0.04 FWHM) Lyot filter, which was built by Lyot and tailored to the CN band at Sacramento Peak in the early 70's.

Results. The presented theoretical computations predict that bright-point contrast in narrow-band (0.04 FWHM) CN filtergrams is more than 3 times higher than in CN filtergrams taken with 1 nm FWHM wide filters, and in typical G-band filtergrams. Images taken through the Lyot filter after optimizing its passband confirm that the filter is capable of rendering small-scale magnetic elements with contrasts that are much higher than in traditional G-band imaging. The filter will be available as an user instrument at the Dunn Solar Tower.

Key words. Techniques: spectroscopic – Sun: photosphere – Sun: magnetic fields – Radiative transfer –Molecular data

1. Introduction

Many Fraunhofer lines weaken in locations where strong small-scale magnetic fields appear outside sunspots and pores. While this weakening manifests itself as gaps in the spectral lines, it produces a local brightening in spectroheliograms produced from line core intensities, and hence provides a convenient method for tracking the small-scale magnetic field without the need to collect polarimetric signals. This property of spectral lines is exploited particularly effectively in G-band imaging, in which typically 1 nm full width at half maximum (FWHM) filters centered on a region of the spectrum around 430.5 nm with many lines of the CH molecule are employed. When the CH lines weaken in magnetic elements, the filter integrated signal increases markedly, providing a high contrast with respect to the surrounding surface in the filter image (Carlsson et al., 2004; Vögler et al., 2005; Uitenbroek & Tritschler, 2006).

A similar opportunity is provided by the spectral region shortward of 388.33 nm which contains many lines of the $\nu = 0 - 0$ CN $B^2\Sigma^+ - X^2\Sigma^+$ system. Since the CN band is further to the blue than the G band, it potentially offers higher spatial resolution because of a smaller Airy disk, and higher contrast rendering of temperature differences, because of the wavelength dependence of the Planck function. Indeed, observations presented by Zakharov et al. (2005) suggest that filtergrams taken through a 0.8 nm FWHM wide filter centered at 387.9 nm provide higher contrast (by a factor of 1.4) in the magnetic elements than through a G-band filter of comparable width (Note that Zakharov et al. (2005) erroneously cite 388.7 nm as the central wavelength of their CN filter.) Theoretical calculations by Uitenbroek & Tritschler (2006), however, find the contrast to be

nearly equal, with the bright points having a slightly lower (by a factor of 0.96) contrast on average in synthetic CN filtergrams calculated from a three-dimensional snapshot of a magnetohydrodynamic simulation of solar convection. This issue has yet to be resolved by comparing additional simultaneous observations in both molecular band passes, and modeling in additional simulation snapshots.

In the present paper we argue that a more appropriate way of utilizing the weakening of CN lines is by imaging the solar surface in the band head proper, rather than through a 1 nm type filter. The band head at 388.33 provides this opportunity because many lines accumulate there and meld into a broad spectral feature, thus allowing a for passband that is much broader than a single CN line. In addition, the signal of a filtergram through a narrow passband centered on 388.3 nm, just blueward of the CN band head, is not affected much by either Doppler shifts in and out of the passband, or by Zeeman splitting of the CN lines.

The usefulness of imaging the solar surface in the CN band head was recognized early on, e.g. Gillespie (1971), Sheeley (1971), but the passband became impractical when CCD detectors with much less sensitivity in the blue started to replace film. Since fast back-illuminated CCDs with sufficient blue sensitivity are becoming more prevalent it is time to investigate the sensitivity of the CN band head intensity to magnetic elements in more detail. In this paper we discuss our efforts to revive an old narrow-band Lyot filter for the CN band head, characterize its transmission profile, and present images taken through the filter at the Dunn Solar Telescope (DST) of the National Solar Observatory in Sacramento Peak. The filter has survived moth-balling for more than 15 years, appears in good state and will be available as an user instrument at the DST. With this effort we hope to make once again available narrow-band imaging in the CN band as a routine technique for studying the behavior of

* Operated by the Association of Universities for Research in Astronomy, Inc. (AURA), for the National Science Foundation

small-scale magnetic field elements at the highest spatial resolution, and with the highest contrast.

This paper is organized as follows. In Section 2 we briefly describe the employed method for generating theoretical synthetic narrow-band filtergrams in the CN band, and make plausible that these have very high contrast in small-scale magnetic features. In Section 3 we describe the narrow-band Lyot filter for 388.3 nm. Observations and the characterization of the filter are presented in Section 4, and conclusions in Section 5.

2. Modeling narrow-band CN filtergrams

We explore the benefits of narrow-band CN imaging in the 388.33 band head with numerical radiative transfer modeling in a snapshot from a three-dimensional magnetohydrodynamic simulation of solar surface convection.

2.1. Method

The method we employ is described in Uitenbroek & Tritschler (2006). The emergent spectrum was calculated at 600 wavelength positions over the range of 386.7 nm to 389.6 nm through a three-dimensional simulation snapshot from a magnetohydrodynamic simulation of solar convection (Stein & Nordlund, 1998). This spectral region includes 327 lines of the CN $B^2\Sigma^+ - X^2\Sigma^+$ system ($v = 0 - 0$, where v is the vibrational quantum number), 231 weak lines ($gf \leq -5$) of the CH $A^2\Delta - X^2\Pi$ system ($v = 0 - 1$ and $v = 1 - 2$), 62 stronger lines of the CH $B^2\Sigma^- - X^2\Pi$ system ($v = 0 - 0$), and the hydrogen Balmer line H_8 between levels $n = 8$ and 2 at $\lambda = 388.905$ nm. We use the same snapshot as before. The emergent spectrum was integrated over filter curves of different widths and position to create synthetic filtergrams. The very good agreement between the mean spectrum, averaged over the surface of the simulation cube, and the observed solar average spectrum (Figure 1) indicates that the simulation and radiative transfer modeling are highly realistic. The biggest discrepancy between synthetic and observed spectra occurs in the wings of the Balmer H_8 line the wings of which are too narrow in the former because no linear Stark broadening was included in the computation. Magnetic concentrations in the resulting filtergrams, shown in Figure 2, stand out as bright ribbon-like features. The average bright-point contrasts for filtergrams synthesized through 1 nm FWHM G-band and CN-band filter curves, and through three narrow-band filters of 0.05, 0.10, and 0.20 nm FWHM are given in Table 1. On average the pixels selected as bright points in the 0.05 nm and 0.10 nm filters, respectively, have more than three and two times higher contrast than in the 1 nm FWHM filtergram, while the 0.20 nm filter only gives an enhancement that is 26% higher. The average bright-point contrast in the synthetic filtergrams was derived in the same manner as described in Uitenbroek & Tritschler (2006), namely by subtracting a certain fraction of a blue continuum filtergram from the synthetic G-band filtergram to eliminate the granulation pattern as much as possible, and then keeping all pixels above a certain threshold in the difference filtergram.

2.2. Explanation for the high narrow-band contrast

Using a response function of the filter-integrated intensity to temperature (Uitenbroek & Tritschler, 2006) pointed out that the brightness enhancement of the magnetic features in 1 nm FWHM filtergrams in the G band and 388.3 nm CN band does not result from relatively higher temperatures compared to the

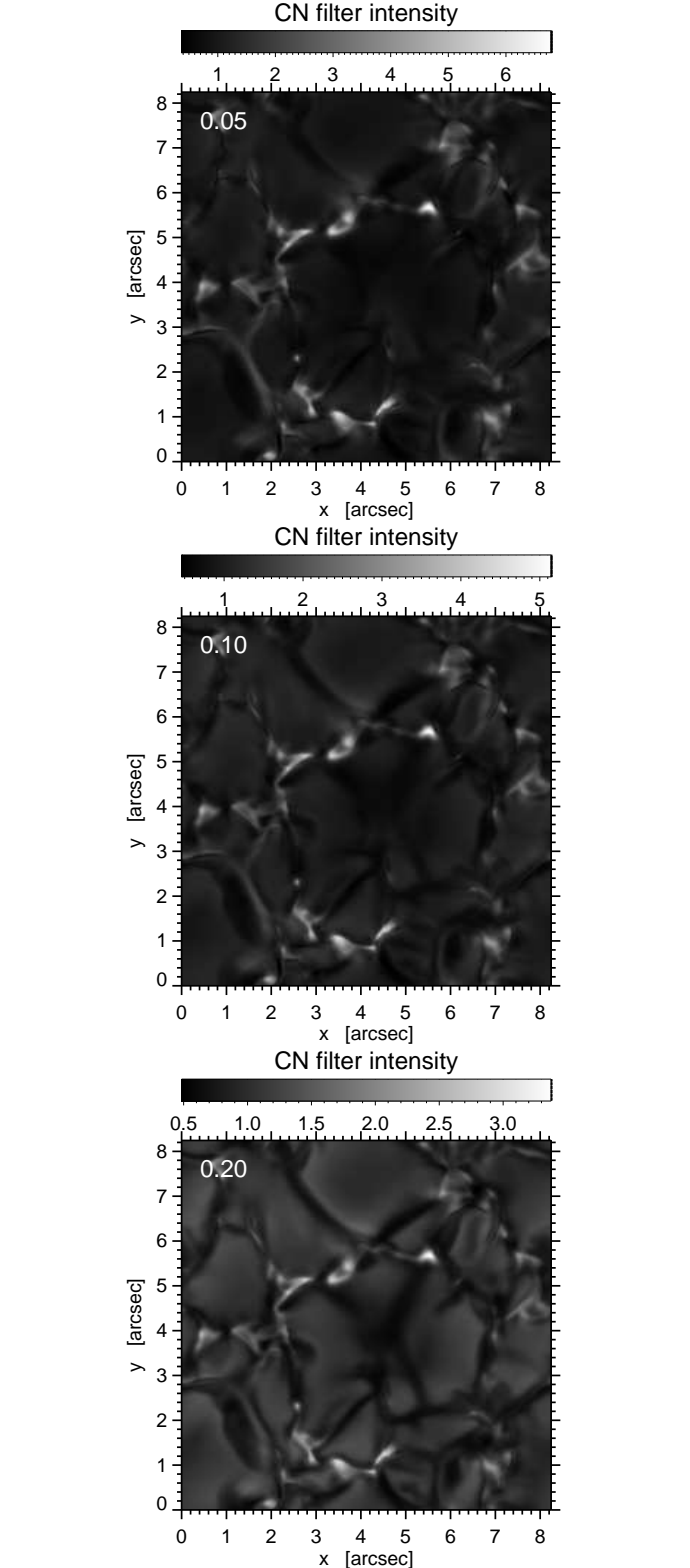


Fig. 2. Synthetic CN-band filtergrams for filters with FWHM of 0.05 nm (top panel) 0.10 nm (middle panel), and 0.20 nm (bottom panel), all three centred on the CN band head at 388.3 nm.

surrounding photosphere, but from the partial evacuation of the regions of highest magnetic flux concentration. To balance the sum of magnetic and gas pressures inside a magnetic field concentration with the gas pressure of the non-magnetic surroundings the internal gas pressure is substantially lower than the ex-

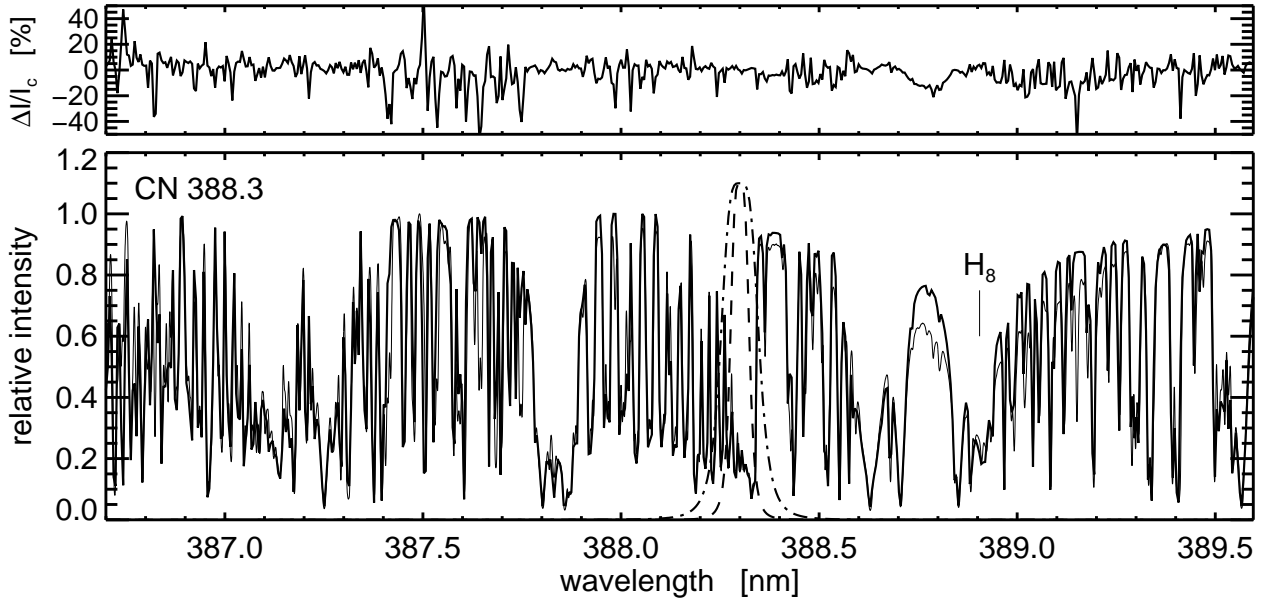


Fig. 1. Comparison of the synthetic spectrum over whole computed range, averaged over the whole surface of the simulation cube, and the observed solar average spectrum. Filter curves for 0.05 and 0.10 nm FWHM passbands centered at 388.3 nm are also shown.

Table 1. Average bright-point contrasts for the G band and wide- and narrow-band CN filter curves

Filter	CWL [nm]	FWHM [nm]	BP contrast
G band	430.5	1.00	0.497
CN 388.3	388.3	1.00	0.478
CN 388.3	388.3	0.05	1.741
CN 388.3	388.3	0.10	1.150
CN 388.3	388.3	0.20	0.602

ternal one at equal geometric height. In the lower pressure environment the density of molecules is reduced resulting in a weakening of the molecular spectral lines for lines of sight that look down into strong magnetic field concentrations. The weakening of spectral lines in the filter passband causes the integrated filter intensity to be higher, leading to the characteristic intensity enhancements of magnetic elements. This brightening-through-evacuation mechanism is wavelength independent resulting in the similar contrasts in the two molecular bands.

In the CN band head, just longward of 388.3 nm, however, many CN lines accumulate. The overlap of these multiple lines causes the formation of intensity over the whole wavelength interval of the band head to appear in higher layers, where it samples higher temperatures, at equal geometric height, than in the surrounding non-magnetic medium because of the shallow temperature gradient in the flux concentration (see Uitenbroek & Tritschler, 2006, their Figure 9). This shallow gradient is the result of inhibition of convective heat flux below the photosphere, and lateral radiative influx just above the photosphere. In similar fashion as most photospheric spectral lines weaken, the raised temperature at the formation height of the lines raises the central intensity of the CN lines in the band head, with additional line weakening due to increased molecular dissociation. Since the line weakening is a direct measure for the temperature at the formation height it is advantageous to observe it at shorter wavelengths, where the response of the

Planck function to temperature is more non-linear. The advantage of the CN band head is that it is a relatively broad feature that requires less narrow filters than a single spectral line, before its filter-integrated intensity becomes contaminated by continuum contributions. The latter only starts to occur for filters of 0.20 nm FWHM, or wider, as is clear in Figure 2 and Table 1.

3. Description of the narrow-band Lyot filter

We do not know much about the origin of the filter, there seems to be no documentation or reports about it. The filter survived languishing in the vaults of the Evans facility at Sacramento Peak. The black metal cover makes it look very similar to an old H α filter that resides also in one of the cabinets at the Evans facility. The face plate of the H α filter indicates by a serial number and a label that it was built by Bernard Lyot himself. Although this face plate is missing for the CN filter we take the similar looks of both filters as an indication that the CN filter also was built by Lyot himself but modified at Sacramento Peak probably by Richard Dunn in the early 70's. Because of missing documentation we have no insight into the *inner life* of the filter in terms how many elements (calcites, polarizers) are used, what the length of the thinnest calcite is, etc., which would be necessary to know in order to model the transmission band. Removing the outer metal cover reveals that the optics is wrapped in cork for protection and to insulate the optics. The thermal control consists of a controller and heating wires underneath the cork wrap, and an additional temperature sensor with an external readout device. Changing the temperature results in a change of central wavelength (CWL) and the shape of the passband: when heated the filter passband moves towards the blue. The entrance polarizer is removable. This disables the thickest element, effectively doubling the width of the passband (e.g. see Stix, 2004). The entrance polarizer can be rotated to align the optical axis of the entrance polarizer and the first calcite element: fast and slow axis of the calcite must be 45° with respect to the entrance polarizer.

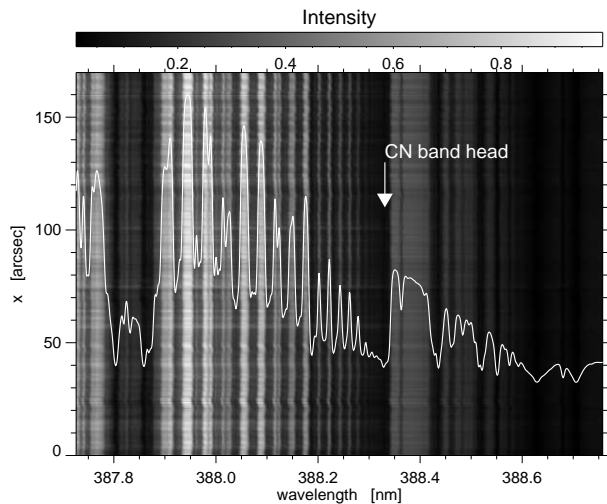


Fig. 3. Sample spectrum of the CN band at 388.33 nm taken with the prefilter only. Overplotted is the averaged spectrum. The CN band head is indicated. The spectrum is not corrected for the prefilter transmission curve.

Rotation of the entrance polarizer (if present) also rotates the exit polarizer.

4. Observations

Between 2006 May 1 and May 6, we performed spectroscopic and imaging observations with the Lyot filter at the Dunn Solar Telescope (DST) of the National Solar Observatory at Sacramento Peak in order to characterize its transmission profiles, and to test its image quality, respectively. We describe these observations below.

4.1. Spectroscopic

The spectroscopic observations presented here have been performed between May 1 and May 4 and were done in two different manners. First, we obtained data to characterize the Lyot filter and its prefilter. Second, we scanned the solar surface by stepping the Horizontal Spectrograph (HSG) in order to generate two-dimensional maps at each wavelength position of the available CN spectrum around 388.33 nm. In the former case the Lyot was placed in front of the slit of the HSG. In both cases the prefilter, needed to eliminate side bands of the Lyot, was mounted directly in front of the camera. The available prefilter was an old interference filter, the passband of which had unfortunately drifted towards the blue (see Sect. 4.4).

Data acquisition was accomplished with a 1024×1024 pixel² detector manufactured by Spectral Instruments (SI 805-205) with a $13 \mu\text{m}$ pixel size. The chip is backside illuminated for enhanced blue sensitivity and has a quantum efficiency of $\sim 70\%$ at the observed wavelength. The integration time was set to 3 s. The dispersion in wavelength direction is $10.1 \text{ m}\text{\AA} \text{ pixel}^{-1}$ and the spatial scale along the slit is $0.171 \text{ arcsec pixel}^{-1}$. Figure 3 shows a spectrum of the wavelength region as seen through the prefilter only. The location of the band head is indicated by the white arrow.

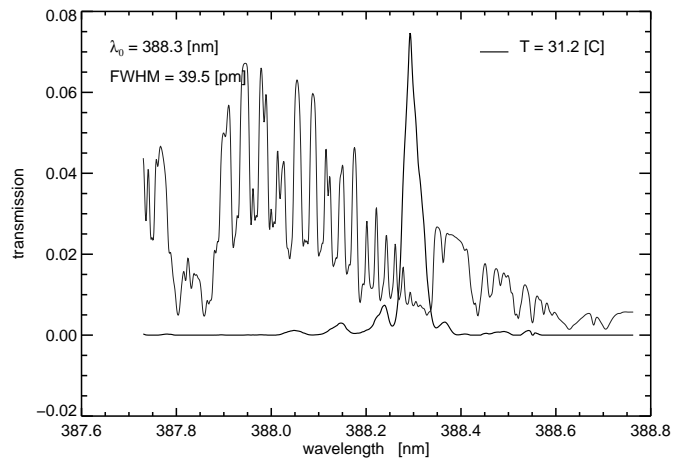


Fig. 4. Optimal passband shape of the CN Lyot filter (*thick curve*). With a CWL of 388.3 nm, just to the blue of the band head at 388.33 nm the width is 0.04 nm (FWHM). Also plotted is the observed spectrum through the prefilter averaged over 32 frames in flatfield mode.

4.2. Characterization of the Lyot passband

To characterize the Lyot filter we recorded data with and without the Lyot in the optical path. In both cases the telescope was run in flatfield mode, moving the pointing randomly over the central part of the solar disk during exposures in order to blur spatial details. Taking the ratio of the average of the 32 spectra spectra each with and without the Lyot allows us to determine the passband of the filter. We obtained the passband in this manner for different temperature settings, ranging from $30.4 \text{ }^\circ\text{C}$ to $33.2 \text{ }^\circ\text{C}$. We found that the passband moves towards the blue with increasing temperature, and splits into two peaks. Interpolating the measured central wavelength versus temperature relation we determined that the temperature setting in which the passband optimally covers the band head without the entrance polarizer present is $31.2 \text{ }^\circ\text{C}$. The passband for this optimal temperature is shown in Figure 4, together with the average spectrum obtained by averaging the 32 disk center spectra taken without the Lyot, but including the prefilter. Fitting a Gaussian curve to the filter transmission shows that the central wavelength is 388.3 nm and the width of the filter is 0.04 nm FWHM. Note that the peak transmission of the filter is almost 8%, confirming its excellent optical condition.

4.3. Passband of the Lyot with entrance polarizer

We also tested the behavior of the Lyot's passband in its narrow setting with the entrance polarizer in place. In particular, we obtained the transmission profile of the filter for different angles of the polarizer, at the optimal temperature setting for the wide passband configuration. Rotating the exit polarizer also rotates the entrance polarizer (and vice versa). The result is shown in Figure 5 for rotation angles from 0° to 350° in steps of 10° . The optimal position of the 0.04 nm passband is displayed for comparison. The best match between the two passbands at a temperature of $31.2 \text{ }^\circ\text{C}$ would be at an angle of 200° or 210° , except for that the narrower passband shows significant side lobes for most of the angles. The cleanest narrow passband occurs for $140\text{--}150^\circ$, but is shifted too far to the blue. Perhaps the latter could be corrected by lowering the operating temperature slightly, but

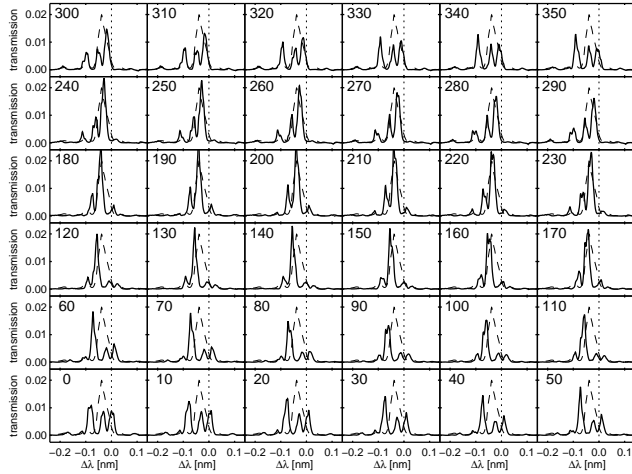


Fig. 5. Variation of the Lyot's passband with rotation angle of the exit polarizing element when the entrance polarizing element is mounted (*thick solid curves*), which means that the passband is ~ 0.02 nm. For comparison we overplot the optimal position of the 0.04 nm passband (entrance polarizing element not mounted, *dashed curve*). Wavelength differences are defined with respect to the band head.

the much reduced peak transmission of only 2% makes this configuration less attractive because of the long exposure times it requires. The wider passband is narrow enough to profit from the contrast properties of the of the CN band head feature, and therefore much more attractive in practice.

4.4. Characterization of the prefilter

For prefilter characterization we removed the Lyot from the optical path and took spectral data with the prefilter placed directly in front of the detector. We took the spatially averaged observed spectrum and divided it by the observed disk center intensity from the FTS atlas by Brault (1978, 1993) as provided by Kurucz¹. This ratio, which is rather uneven because of small wavelength offsets and differences in spectral broadening between the two, is plotted with the thin curve in Figure 6. To get a proper estimate of the CWL and width of the prefilter's band pass we fitted a Gaussian curve to the ratio (*thick curve* in Figure 6), and found values of 387.9 nm and 0.89 nm (FWHM), respectively. From this it is clear that the CWL is, unfortunately, too far in the blue and not centered on the CN band head, and therefore, makes exposure times longer than necessary. Tilting the prefilter would not alleviate this problem as it moves the passband even further towards the blue.

4.5. Two-dimensional spectral maps

One possible way to test the image quality of the filter is to construct CN band head spectroheliograms by integrating observed spectra over the determined filter passband, and comparing these to imaging observations through the filter. To this end we generated two-dimensional maps by scanning the spectrograph slit over the solar surface. This was done without the Lyot but with the prefilter in the beam. We scanned areas of 50 arcsec in steps of 0.25 arcsec for a total of 200 steps. The spectra were taken

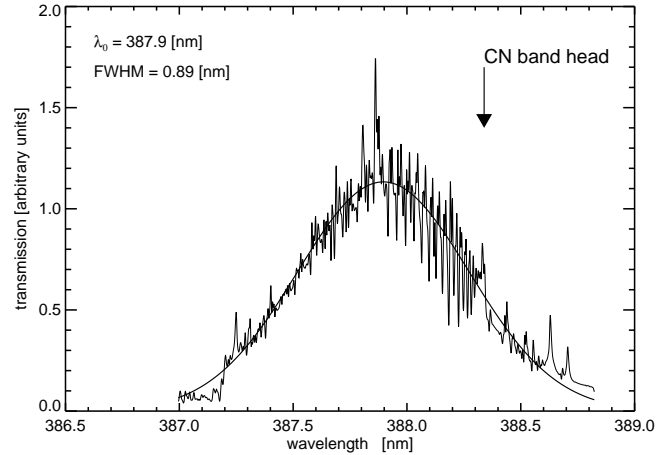


Fig. 6. Ratio of the average observed spectrum with the FTS atlas spectrum (*thin curve* representative of the prefilter transmission profile. the thick curve is a Gaussian fit to the ratio.

with an exposure time of 3 s and a cadence of 5 s. The same wavelength range and dispersion was used as for the observations characterizing the Lyot and prefilter.

On May 2nd, 2006, we scanned across active region NOAA 10879 at N 14.9 and E 10.6. (the region was assigned a number only on the next day). On May 4th, 2006, we scanned across the same active region now at N 15.2 and E 15.9. Figure 7 shows area maps from May 4th for three different wavelength integrations: the CN band head integrated over the passband of the Lyot filter (*top panel*), the core of the CN line at 388.10 nm (*middle*), and the continuum at 387.945 nm (*bottom*). The top two panels clearly show the equivalence of the intensity information obtained in the core of a single CN line and in the integrated band head. It is only the width of the latter that makes it much more practical for filtergram observations. Since we do not have co-temporal G-band images for the spectral scans we cannot construct a mask from such filtergrams to compute the average bright-point contrast. However, if we assume that the theoretical prediction that the average bright-point contrast is almost the same in 1 nm CN band filtergrams as in the G-band, then we can integrate the observed spectra over a 1 nm FWHM filter function, and derive a mask from the resulting spectroheliogram. We find that the average CN bright-point contrast in a 1 nm FWHM filter calculated in this manner is 0.14, while that through the optimal passband of the Lyot is 0.38, almost three times as high as through the wider filter, and in reasonable agreement with the predicted ratio (see Table 1). The observed contrasts are much lower than the predicted ones because of image blurring by unfavorable seeing, beyond what could be corrected by the Adaptive Optics system of the DST.

4.6. Narrow-band filtergrams

We observed region NOAA 10879 at N 15.6 W 1.6. on May 4th, 2006 with the filter in an imaging setup. The exposure time was set to 1 s with the same detector as for the spectroscopic observations. The prefilter was placed in front of the Lyot filter, which itself was placed in an F/36 beam with an intermediate focal plane just after the exit window of the Lyot. Two reimaging lenses were used to bring the final image scale to 0.0474 arcsec pixel⁻¹, which is equivalent to 3.65 arcsec mm⁻¹ an almost identical to

¹ <http://kurucz.cfa.harvard.edu/sun/KPNOPRELIM>

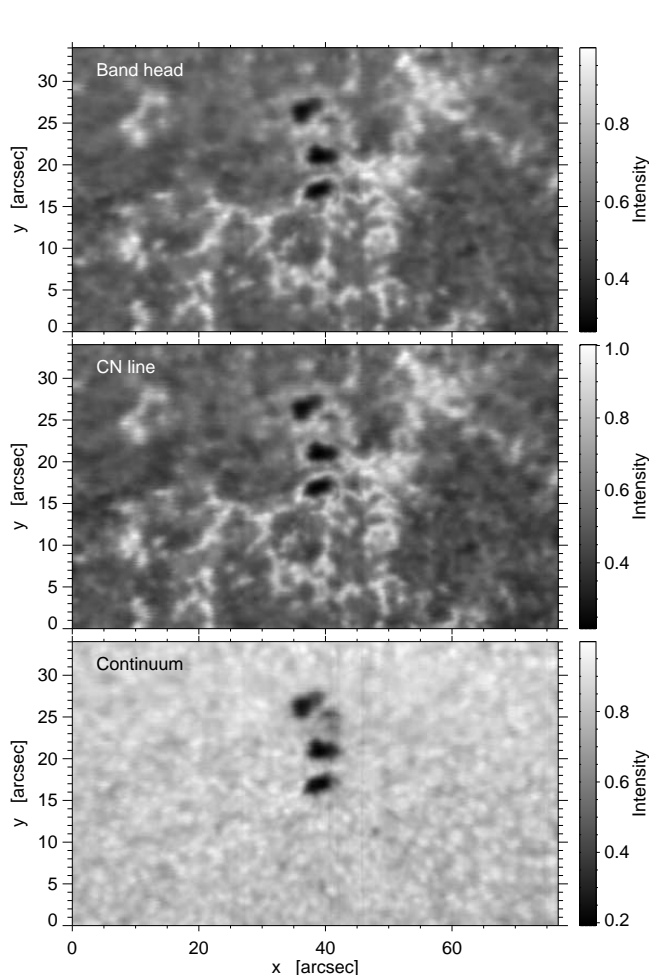


Fig. 7. Area maps of active region NOAA 10879 at N 15.2 and E 15.9 observed on May 4, 2006. Top: in the CN band head. Middle: in the line core of one of the CN lines at 388.10 nm. Bottom: in the continuum at 387.945 nm. The intensity is scaled to the maximum intensity in the map at that wavelength.

that in the telescope’s prime focus. This resulted in a field-of-view (FOV) of 48×48 arcsec.

Note the close similarity between the filtergram in Figure 8 and the heliograms in the CN band head and CN line intensity (Figure 7, *top* and *middle panels*, respectively). We also note the resemblance with filtergrams in the Ca II H and K lines (e.g., Rouppe van der Voort et al., 2005, their Figure 2), which represent, however a slightly higher layer of the atmosphere. In both cases the contrast of small-scale magnetic elements is much higher than in the 1 nm wide G-band filtergrams that are typically used to identify flux concentrations, and allows us to use CN filtergrams as a better proxy for observing small-scale magnetic flux concentrations even when the seeing conditions are not in favor.

5. Conclusions

Given the very similar contrast in the two molecular bands at 430.5 nm and 388.3 nm, it would seem logical to conclude that imaging in the CH band is still the preferred method to track small-scale magnetic fields because of higher detector sensitivity at the longer wavelength. Experimenting with the width and central wavelength of the filter function in the simula-

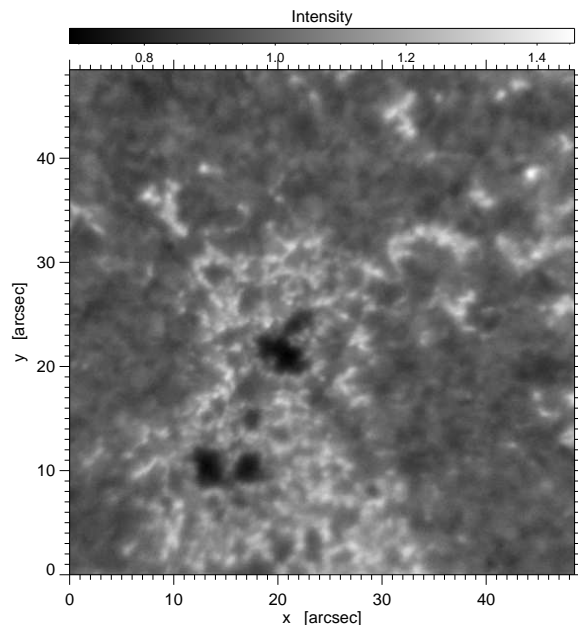


Fig. 8. Image taken centered on the CN rotation band at 388.33 nm with a passband width of ~ 0.04 nm (FWHM). The temperature was set to 31.2 °C.

tions, however, we confirm theoretically that the contrast in the CN band can be greatly enhanced by making the filter narrow (0.05 – 0.2 nm), and centering it directly in the band head at 388.33 nm, a fact known experimentally already in the early seventies. Examples of synthetic filtergrams made with narrow filters of widths 0.05 nm to 0.20 nm shown in Figure 2 and the corresponding average bright-point contrasts listed in Table 1 illustrate this finding.

The simulations also allow us to understand the high contrasts in the narrow-band filtergrams, as outlined in Section 2.2. In the band head the emergent intensity originates from slightly higher (by about 100-200 km) layers and “feels” the temperature enhancement that results from lateral irradiation into the slender flux tubes. This observing mode therefore favors short wavelengths, because it preferentially brings out the higher temperature contrast. The properties of the intensity signal in the CN band head are not different that those in the core of a single CN line (as illustrated in Figure 7), observing in the band head is easier to accomplish because it does not require an extremely narrow filter.

We tested an old Lyot filter suitable for observations in the CN band head and determined its passband with spectroscopic observations at the DST of the NSO at Sacramento peak in May 2006. We found the filter in very good optical condition, and determined that its passband at optimal setting has a width of 39.5 pm (FWHM) and a peak transmission of 7.5% (Figure 4). To achieve this setting the filter has to be operated at an internal temperature of 31.2 C and without its entrance polarizer, disabling the first birefringent element. Theoretically, by constructing synthetic filtergrams from a magneto-hydrodynamic simulation snapshots with the optimal filter shape, we expect very high contrasts of small-scale magnetic features. Figure 9 shows such a filtergram. The average bright-point contrast computed with a bright-point mask derived from G-band brightness as described in Section 2 is 1.937.

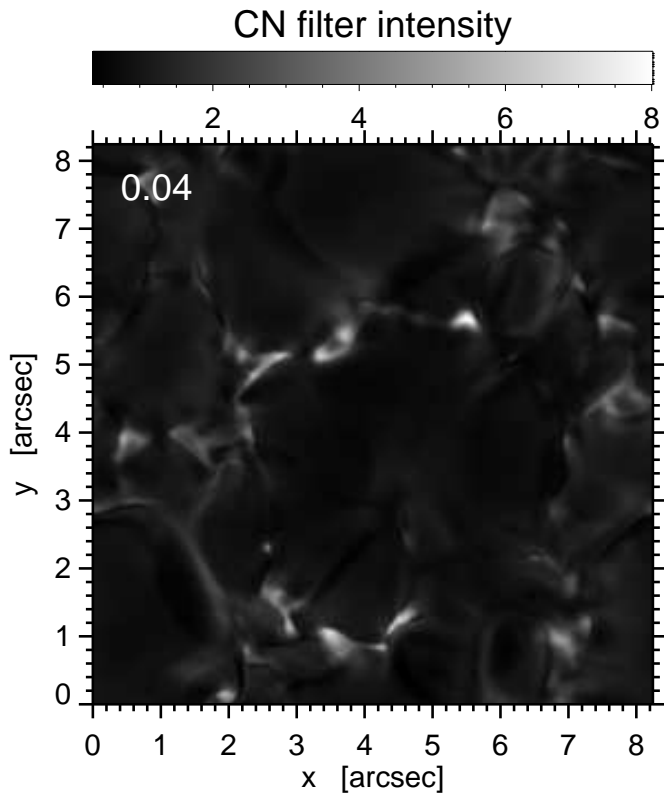


Fig. 9. Filtergram constructed from the theoretical spectrum using the measured filter profile (Figure 4) at the optimal temperature of 31.2 °C.

A sample image taken through the Lyot filter is shown in Figure 8. Because this image was taken under very moderate seeing conditions, and a fairly long exposure time, necessary because of the off-band prefilter (see Section 4.4), the contrast is not very high. Yet, because of the very intrinsic contrast of the bright points they are distinctly visible in the narrow-band CN image, while they would be very hard to detect with a wider passband of 1 nm, or through a typical G-band filter. Comparison of spectro-heliograms constructed with different filter widths from our observed spectra confirm our theoretical findings that a 0.05 nm FWHM filter centered at 388.3 nm provides approximately a threefold enhancement of bright-point contrast over a 1 nm FWHM filter in either the CN band or the G band (Section 4.5).

We conclude that the Lyot filter is a very valuable instrument that is in surprisingly good condition. To increase the throughput and shorten exposure times a new prefilter centered on 388.3 nm has been ordered. With this in place the filter will be available as an user instrument at the DST, and will reenale exploitation of the CN band as a valuable window for monitoring small-scale magnetic field structure and evolution.

Acknowledgements. The authors would like to thank the observers, technicians and engineers who made these observations possible. Particularly Doug Gilliam who remembered the existence of the filter and thus prevented it from further languishing in the vaults of the Evans facility.

References

- Brault, J. W. 1978, in Future solar optical observations needs and constraints, 33
 Brault, J. W. 1993, Solar Fourier transform spectroscopy (in Future Solar Optical Observations Needs, and Constraints 1978) (Selected Papers on Instrumentation in Astronomy), 273

- Carlsson, M., Stein, R. F., Nordlund, Å., & Scharmer, G. B. 2004, ApJ, 610, L137
 Gillespie, B. 1971, Sol. Phys., 21, 93
 Rouppe van der Voort, L. H. M., Hansteen, V. H., Carlsson, M., et al. 2005, A&A, 435, 327
 Sheeley, N. R. 1971, Sol. Phys., 20, 19
 Stein, R. F. & Nordlund, Å. 1998, ApJ, 499, 914
 Stix, M. 2004, The Sun: an introduction (Astronomy and astrophysics library, Berlin: Springer, 2004. ISBN: 3540207414)
 Uitenbroek, H. & Tritschler, A. 2006, ApJ, 639, 525
 Vögler, A., Shelyag, S., Schüssler, M., et al. 2005, A&A, 429, 335
 Zakharov, V., Gandorfer, A., Solanki, S. K., & Löfdahl, M. 2005, A&A, 437, L43